

Article

# Novel Red-Emitting $\text{Eu}^{3+}$ -Doped $\text{Y}_2(\text{W}_x\text{Mo}_{1-x}\text{O}_4)_3$ Phosphor with High Conversion Efficiency for Lighting and Display Applications

Fan Chen, Muhammad Nadeem Akram and Xuyuan Chen \* 

Department of Microsystems, Faculty of Technology, Natural Sciences and Maritime Sciences, Campus Vestfold, University of South-Eastern Norway, 3184 Borre, Norway; chenfan13571038693@163.com (F.C.); muhammad.n.akram@usn.no (M.N.A.)

\* Correspondence: xuyuan.chen@usn.no; Tel.: +47-31-00-90-28

**Abstract:** In this study, a series of trivalent europium-doped tungstate and molybdate samples were synthesized using an improved sol-gel and high-temperature solid-state reaction method. The samples had different W/Mo ratios and were calcined at various temperatures ranging from 800 to 1000 °C. The effects of these variables on the crystal structure and photoluminescence characteristics of the samples were investigated. It was found that a doping concentration of 50% for europium yielded the best quantum efficiency based on previous research. The crystal structures were found to be dependent on the W/Mo ratio and calcination temperature. Samples with  $x \leq 0.5$  had a monoclinic lattice structure that did not change with calcination temperature. Samples with  $x > 0.75$  had a tetragonal structure that remained unchanged with calcination temperature. However, samples with  $x = 0.75$  had their crystal structure solely dependent on the calcination temperature. At 800–900 °C, the crystal structure was tetragonal, while at 1000 °C, it was monoclinic. Photoluminescence behavior was found to correlate with crystal structure and grain size. The tetragonal structure had significantly higher internal quantum efficiency than the monoclinic structure, and smaller grain size had higher internal quantum efficiency than larger grain size. External quantum efficiency initially increased with increasing grain size and then decreased. The highest external quantum efficiency was observed at a calcination temperature of 900 °C. These findings provide insight into the factors affecting the crystal structure and photoluminescence behavior in trivalent europium-doped tungstate and molybdate systems.

**Keywords:**  $\text{Eu}^{3+}$  doped; red phosphor; quantum efficiency; thermal quenching; laser lighting



**Citation:** Chen, F.; Akram, M.N.; Chen, X. Novel Red-Emitting  $\text{Eu}^{3+}$ -Doped  $\text{Y}_2(\text{W}_x\text{Mo}_{1-x}\text{O}_4)_3$  Phosphor with High Conversion Efficiency for Lighting and Display Applications. *Molecules* **2023**, *28*, 4624. <https://doi.org/10.3390/molecules28124624>

Academic Editors: Giuseppe Cirillo, Tomasz Sadowski and Guankui Long

Received: 21 May 2023

Revised: 5 June 2023

Accepted: 6 June 2023

Published: 7 June 2023



**Copyright:** © 2023 by the authors. Licensee MDPI, Basel, Switzerland. This article is an open access article distributed under the terms and conditions of the Creative Commons Attribution (CC BY) license (<https://creativecommons.org/licenses/by/4.0/>).

## 1. Introduction

Solid-state lighting (SSL) technology has emerged as a major contender in the field of artificial lighting, replacing traditional incandescent and fluorescent lamps due to its advantages in terms of high efficiency, small size, longer life span, cost-effectiveness, and eco-friendliness [1–6]. The key component of this technology is the white light-emitting diode (WLED), which is fabricated using inorganic semiconductor electro-optical conversion chips [7–9]. Two primary approaches are used for generating white light: one based entirely on semiconductor chips, and another utilizing semiconductor chips along with wavelength conversion materials (phosphors) [10–12]. In the former approach, LED chips of different colors (wavelengths) are mixed to produce white light. The latter method involves coating blue or near-ultraviolet (NUV) LEDs with a phosphor that absorbs and converts blue/NUV light into visible light of a different wavelength, which is then combined to generate white light [13]. The first commercially available LED plus wavelength-conversion material method utilized a blue-emitting GaN-based LED chip combined with a yellow-emitting phosphor (YAG:  $\text{Ce}^{3+}$ ) to create white light [14]. However, this approach has certain limitations, primarily a low color rendering index (CRI), particularly in R9 (usually

negative) that represents red, owing to the absence of red components in the resulting white light spectrum [15,16]. To enhance CRI, a mixture of different phosphor materials is typically employed; specifically, red-emitting phosphors are added to yellow-emitting phosphors [17,18]. Thus, extensive research efforts have been directed towards the development of high-quality and cost-effective red phosphor materials [19,20].

Rare-earth ions are commonly used as the luminescence center of red-emission materials, with  $\text{Sm}^{3+}$ ,  $\text{Eu}^{3+}$ ,  $\text{Tb}^{3+}$ , and  $\text{Dy}^{3+}$  being the most prevalent.  $\text{Eu}^{3+}$  is particularly known for its intense emission, high efficiency, and saturated red color [6,21,22]. The electronic configuration of  $\text{Eu}^{3+}$  can be expressed as  $[\text{Xe}]4f^6$ , with 54 electrons in the same closed shell as the xenon atom and 6 electrons in the 4f shell [23]. The 4f shell is located within the closed  $5s^2$  and  $5p^6$  shells and is adequately shielded from the crystal field environment. This leads to a largely unaffected energy level distribution of the 4f shell by an external environment. Molybdates and tungstates are classic host materials for  $\text{Eu}^{3+}$ -doped red-emission phosphor materials, extensively studied by scientific researchers. Due to having similar chemical properties and physical structures, Mo and W can be doped into each other's group ( $[\text{MoO}_4]^{2-}$  and  $[\text{WO}_4]^{2-}$ ) without any changes to the crystal structure [24–27]. However, the crystal lattice parameters and the internal stress of the mixed structure,  $(\text{Mo}/\text{WO}_4)^{2-}$ , could vary slightly due to the difference in size of  $\text{Mo}^{6+}$  and  $\text{W}^{6+}$  ions. Depending on the synthesis conditions, such as calcination temperature and pressure, different types or mix of crystalline structures, such as monoclinic (C2/c), orthorhombic (Pba2, Pbcn), and tetragonal ( $\text{P}\bar{4}2_1\text{m}$ ), could possibly be created in the material.

Yttrium molybdate, as the main material of trivalent europium, has been reported multiple times [28–30]; in order to further improve the photoluminescence performance of this type of powder material, we replaced some molybdenum atoms with tungsten atoms to form a new host material,  $\text{Y}_2(\text{W}_x\text{Mo}_{1-x}\text{O}_4)_3$ . In this study, a series of  $\text{Eu}^{3+}$ -doped  $\text{Y}_2(\text{W}_x\text{Mo}_{1-x}\text{O}_4)_3$  phosphors were successfully synthesized using improved sol-gel and high-temperature solid-state reaction methods. The impact of synthesis temperature and Mo/W ratio on the lattice structure was assessed, together with the photoluminescence performance of samples with different lattice structures. The novel red phosphor  $\text{Eu}^{3+}:\text{Y}_2(\text{W}_x\text{Mo}_{1-x}\text{O}_4)_3$  presented excellent photoluminescence performance, particularly in terms of luminescence intensity and thermal quenching temperature, making this material suitable for improving the color rendering index of white LEDs.

## 2. Results and Discussion

### 2.1. Morphology and Particle Size by Scanning Electron Microscopy

The present study investigates the particle size and microscopic morphology of synthesized  $\text{Eu}^{3+}$ -doped tungstate/molybdate red phosphor powder. Scanning electron microscopy (SEM) was utilized to obtain the SEM images of  $\text{Y}_2(\text{W}_x\text{Mo}_{1-x}\text{O}_4)_3$  ( $x = 0, 0.25, 0.50, 0.75,$  and  $1.0$ ) samples calcined at different temperatures (800 °C, 900 °C, and 1000 °C). The SEM images revealed that the powder particles have a homogenous particle size, irregular near-round or oval-shaped grains, and a clear grain boundary with some agglomerations, as shown in Figure 1. The particle size is observed to be influenced by the combined effect of calcination temperature and  $x$  value. At a calcination temperature of 800 °C, the particle size remains constant at around 0.5  $\mu\text{m}$  regardless of the variation in  $x$  value. Conversely, when the calcination temperature is greater than 800 °C, the particle size significantly increases with the increase in Mo content, ranging from 0.7 to 3  $\mu\text{m}$  (900 °C) and from 1 to 5  $\mu\text{m}$  (1000 °C).

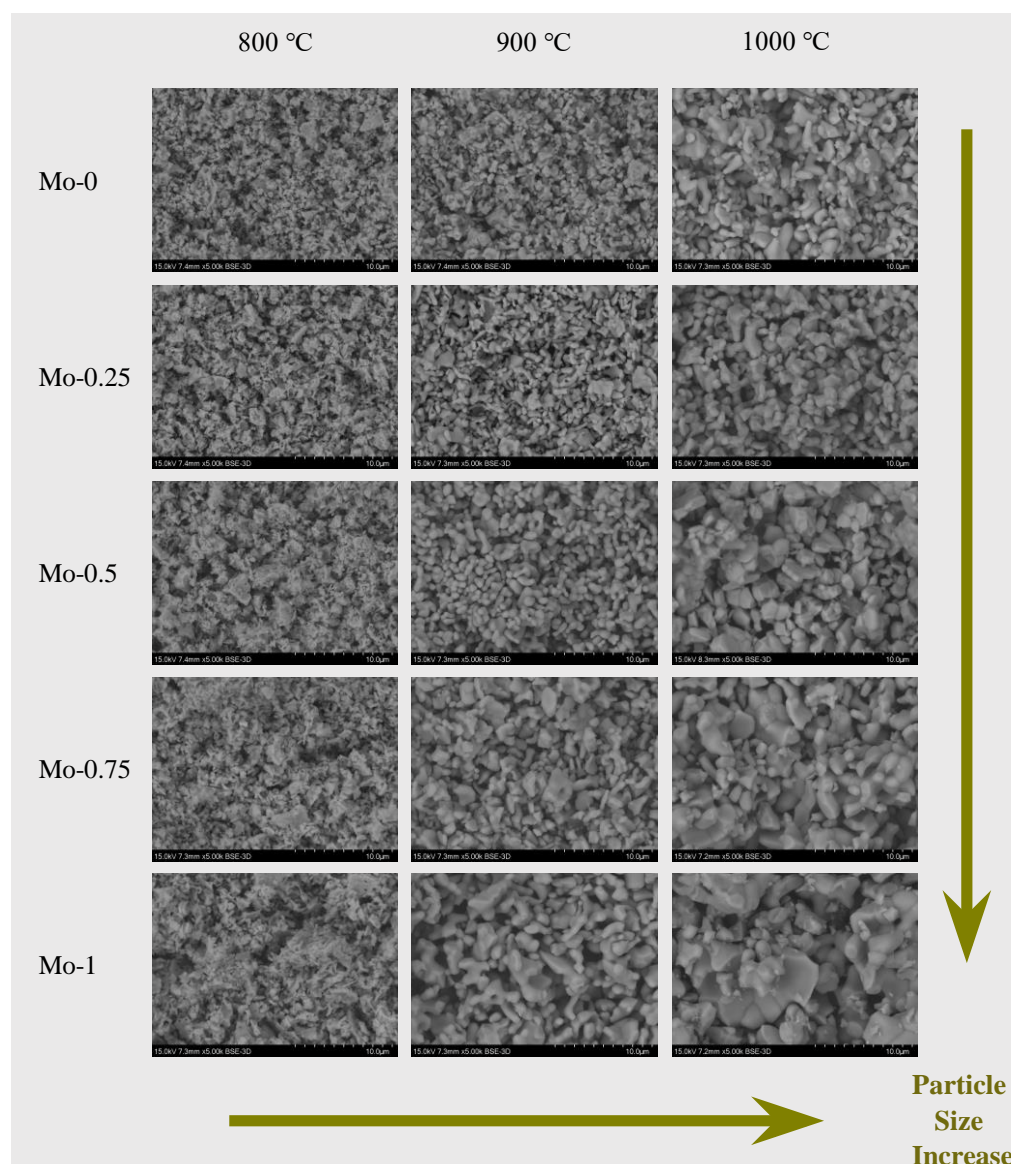
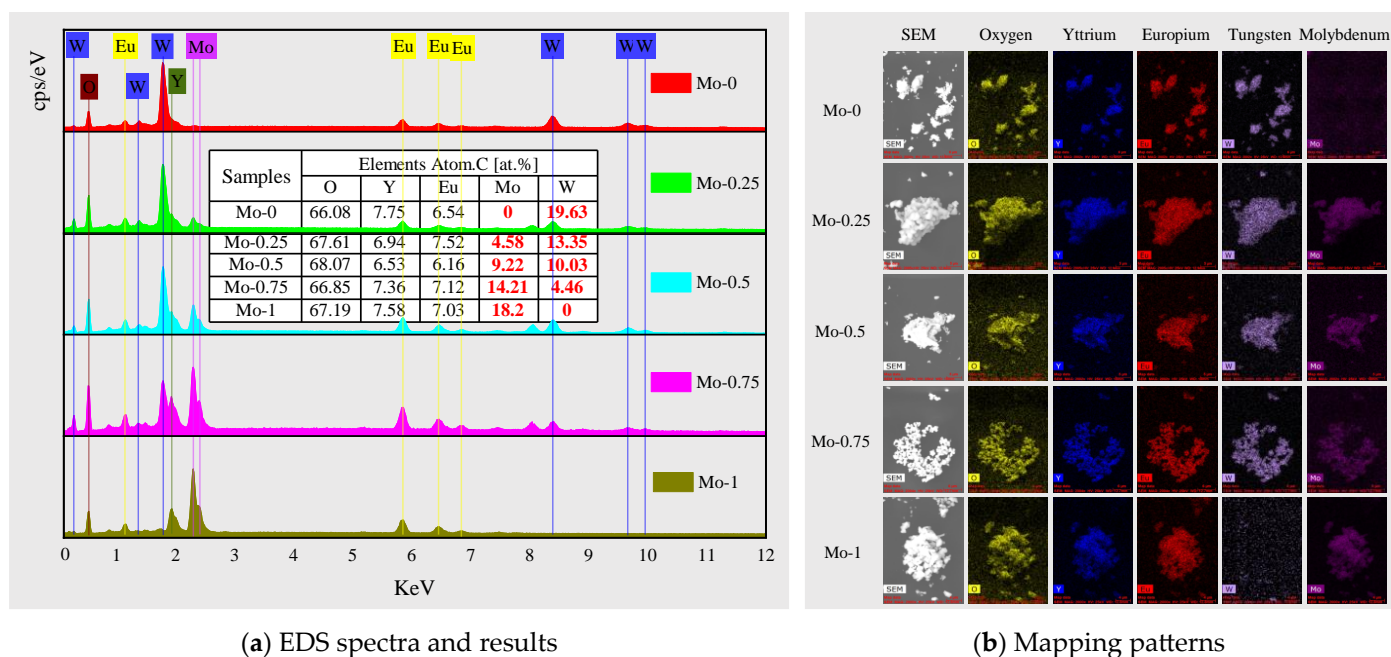


**Figure 1.** SEM images of samples at different calcination temperatures and different Mo/W ratios.

## 2.2. Component Identification by Energy Dispersive Spectrometer

The elemental composition and proportion of each component were analyzed and confirmed through energy-dispersive spectroscopy (EDS), as presented in Figure 2a. The interpolation table displays the percentage of atomic relative quantity of each element in each sample. In this research,  $\text{Eu}^{3+}$  was used as the luminescent center and was doped into  $\text{Y}_2(\text{W}_x\text{Mo}_{1-x}\text{O}_4)_3$  ( $x = 0, 0.25, 0.50, 0.75, \text{ and } 1.0$ ) host material to replace half of the yttrium atom position, such that the  $\text{Eu}^{3+}$  doping concentration was expected to be 5.9 mol%. Based on the EDS results, the molar concentration of  $\text{Eu}^{3+}$  doping is 6–7%, slightly higher than the design value of 5.9%. However, this error falls within the typical error range of EDS for element content measurement; thus, the EDS measurement results are reliable. The manual shielding of the detected carbon peak during quantitative analysis of EDS leads to a slightly higher content of other elements. The  $x$  value was calculated based on the molybdenum and tungsten content measured by EDS, and these values (0, 0.255, 0.479, 0.761, and 1) were found to be close to the design value, confirming the successful synthesis of a series of  $\text{Eu}^{3+}$ -doped  $\text{Y}_2(\text{W}_x\text{Mo}_{1-x}\text{O}_4)_3$  ( $x = 0, 0.25, 0.50, 0.75, \text{ and } 1.0$ ) red-emitting materials. The EDS mapping patterns in Figure 2b support this finding.



(a) EDS spectra and results

(b) Mapping patterns

**Figure 2.** EDS energy spectra (a) and mapping patterns (b) of samples with different Mo content at 900 °C calcination temperature; the table in figure (a) shows element content of each sample.

### 2.3. Crystal Structures and XRD Patterns

Trivalent yttrium/europium molybdates and tungstates belong to the  $RE_2(MO_4)_3$  family and can adopt three distinct crystal structures, which are influenced by composition and synthesis temperature [31–34]. These include the monoclinic  $C12/c1$  space group of the high-temperature  $\beta$  phase, the tetragonal  $P\bar{4}2_1m$  space group of the high-temperature  $\alpha$  phase, and the orthorhombic  $Pba2/Pbcn$  space group of the metastable  $\beta'$  phase [28,29]. Moisture content during the synthesis process also affects the crystal structure, particularly in the  $Pba2/Pbcn$  phase. Studies show that  $Pbcn$  with six coordination is kinetically favored over  $Pba2$  with seven coordination, but exposure to humid environments or annealing below 550 °C can transform  $Pbcn$  into  $Pba2$  due to its thermodynamic and hygroscopic stability [30,35].

To investigate the luminescent properties of  $Y_2(MoO_4)_3$ , we synthesized it using the method described in Section 3.1 to ultimately form the tetragonal  $P\bar{4}2_1m$  space group. Trivalent europium serves as the red luminescent center and replaces half of the trivalent yttrium ions. Our XRD results showed that doping  $Eu^{3+}$  did not alter the crystal structure, nor did calcination at different temperatures. To improve luminescence, we replaced some molybdenum with tungsten to form  $[W_xMo_{1-x}O_4]^{2-}$  ( $x = 0, 0.25, 0.50, 0.75, \text{ and } 1.0$ ). Our XRD diffraction pattern in Figure 3, shows that increasing the proportion of  $W^{6+}$  atoms replacing  $Mo^{6+}$  can lead to a change in crystal structure from tetragonal to monoclinic. This concentration was influenced by calcination temperature, where the  $W^{6+}$  concentration causing crystal change was 0.5 below 1000 °C and 0.25 at 1000 °C. Figure 4 shows the crystal structure's change with the increase in  $W^{6+}$  content, while calcination temperature remains below 1000 °C.

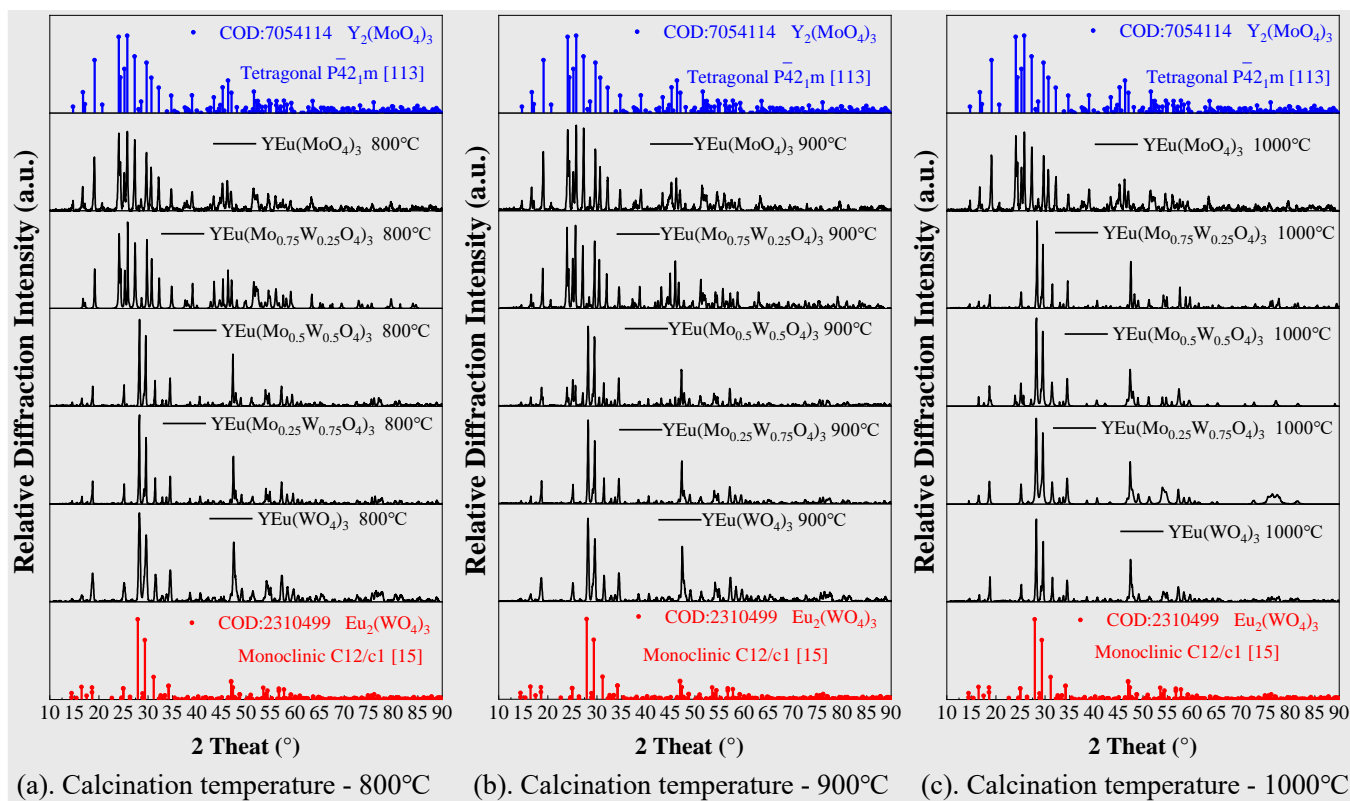


**Figure 3.** XRD diffraction patterns of the samples at different calcination temperatures with different ratios of Mo/W ((a) 800 °C, (b) 900 °C and (c) 1000 °C).

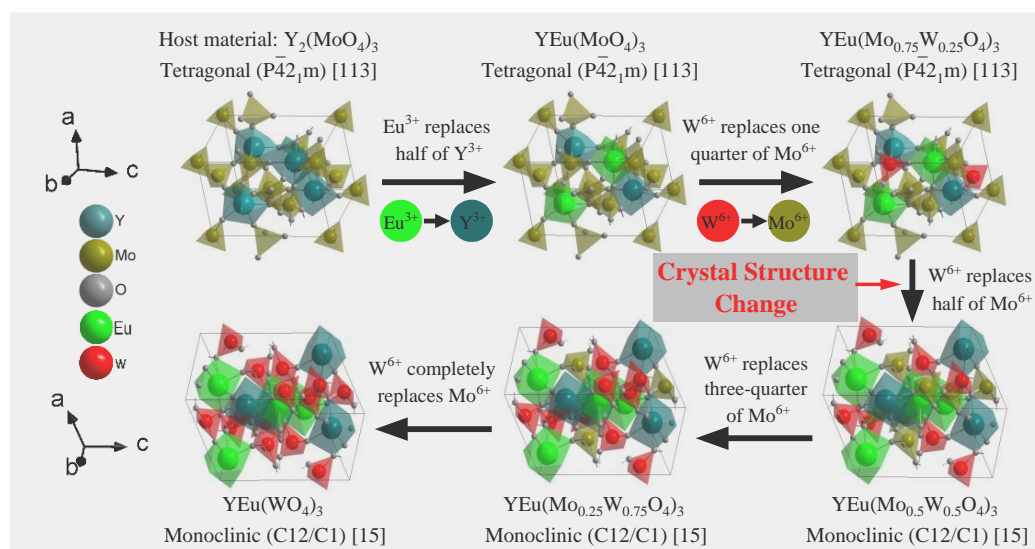


**Figure 4.** The crystal structure of the sample changes with the variable composition at 800 and 900 °C calcination temperature.

#### 2.4. Excitation and Emission Spectra

The present study investigates the excitation and emission spectra of  $Eu^{3+}$ -doped  $Y_2(W_xMo_{1-x}O_4)_3$  ( $x = 0, 0.25, 0.50, 0.75,$  and  $1.0$ ) at room temperature. Excitation spectra were examined at an emission wavelength of 616 nm, while emission spectra were observed under an excitation wavelength of 465 nm. The results reveal that the calcination temperature does not influence the relative excitation and emission spectra. Therefore, analysis was restricted to the sample with a calcination temperature of 900 °C. It is well

established that the excitation spectrum of  $\text{Eu}^{3+}$ -doped red emission material comprises an intense broad band at 230–350 nm due to the charge transfer from ligand ( $\text{O}^{2-}$ ) to metal ( $\text{Eu}^{3+}$  and  $\text{Mo}^{6+}$ ) and many sharp lines at 350–500 nm, ascribed to typical  $\text{Eu}^{3+}$  electron transition 4f-4f. However, the ultraviolet broadband excitation peak is seldom applicable in practical applications because of the large release of heat during the Stokes shift. Therefore, the present study focuses on the narrow-band excitation peaks of  $\text{Eu}^{3+}$  and carefully distinguishes the energy level transitions of each excitation peak, as depicted in Figure 5.

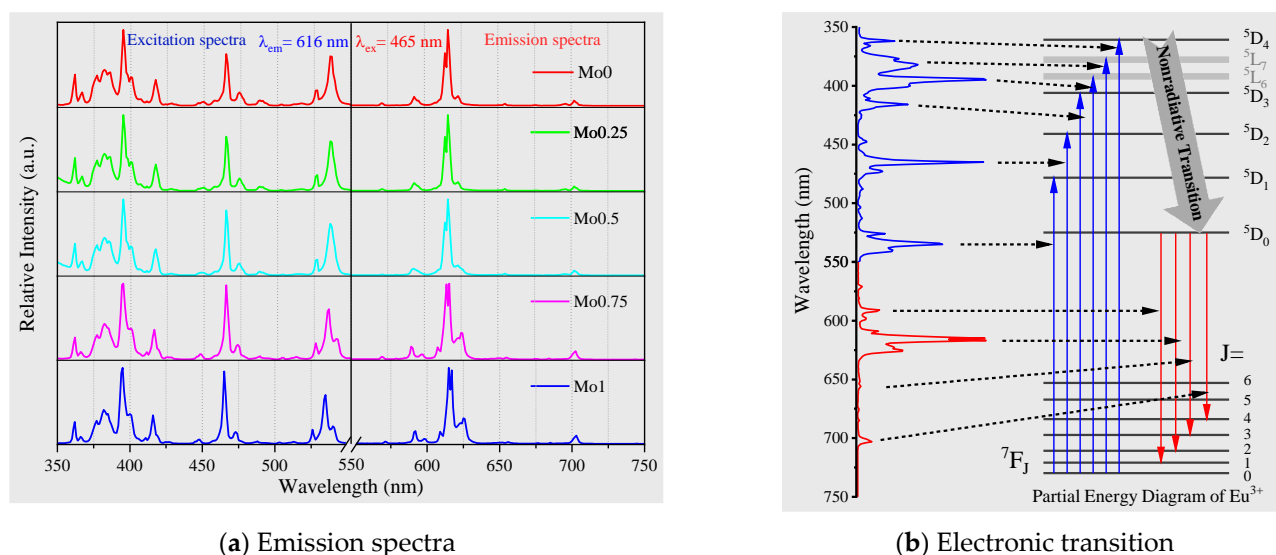


**Figure 5.** Excitation and emission spectra comparison of samples at the same calcination temperature (900 °C) and different Mo/W ratios (a). Correspondence between emission spectrum and electronic transition (b).

The present study highlights the photoluminescence spectra of the characteristic f-f transition in the  $4f^6$  configuration of  $\text{Eu}^{3+}$  ion in the compound, as illustrated in Figure 5a, divided into excitation spectrum and emission spectrum. The narrow excitation peak, ranging from 350 nm to 550 nm, originates from the electronic transitions of  $\text{Eu}^{3+}$  from  $^7\text{F}_0$  ground state to various excited states, viz.,  $^5\text{D}_4$  (360 nm),  $^5\text{L}_7$  (380 nm),  $^5\text{L}_6$  (395 nm),  $^5\text{D}_3$  (415 nm),  $^5\text{D}_3$  (465 nm), and  $^5\text{D}_1$  (535 nm) [36–38]. Among them,  $^7\text{F}_0 \rightarrow ^5\text{L}_6$  (395 nm) and  $^7\text{F}_0 \rightarrow ^5\text{D}_3$  (465 nm) exhibit strong excitation intensity, which synchronizes adequately with the output wavelength of near-UV and blue LED/LD chips produced on a large scale [39,40]. The emission spectra are situated in the 550–750 nm range, found to be linear in spectrum and correspond to the electronic transitions of  $\text{Eu}^{3+}$  from  $^5\text{D}_0$  to  $^7\text{F}_1$ ,  $^7\text{F}_2$ ,  $^7\text{F}_3$ , and  $^7\text{F}_4$  [41–43]. The ratio of the integrated area of the emission peaks corresponding to the  $^5\text{D}_0 \rightarrow ^7\text{F}_2$  and  $^5\text{D}_0 \rightarrow ^7\text{F}_1$  transitions is calculated to be around 7.8, so it can be concluded that  $\text{Eu}^{3+}$  is at a very low symmetry site in the system [44,45]. The most prominent emission peak is  $^5\text{D}_0 \rightarrow ^7\text{F}_2$  (616 nm), which appears as a dazzling red color.

## 2.5. Quantum Efficiency

In the context of evaluating the photoluminescence intensity and heating situation in phosphor materials, quantum efficiency stands as a crucial criterion. We conducted a measurement of the quantum efficiency of the  $\text{Eu}^{3+}$ -doped  $\text{Y}_2(\text{W}_x\text{Mo}_{1-x}\text{O}_4)_3$  ( $x = 0, 0.25, 0.50, 0.75, \text{ and } 1.0$ ) samples at room temperature. The measurement was carried out utilizing a 465 nm laser diode, a calibrated spectrometer, and a standard integrating sphere. As part of the process, we measured and calculated the number of excited light photons emanating from the excitation light source, the number of photons absorbed by the sample,

and the number of photons emitted by the sample. Quantum efficiency was computed via the utilization of the following formulae, i.e., Formula (1) and (2).

$$\eta_{IQE} = \frac{\int R_{Emit}}{\int B_{Abs}} \quad (1)$$

$$\eta_{EQE} = \frac{\int R_{Emit}}{\int B_{Provid}} \quad (2)$$

The calculation requires the determination of  $\int R_{Emit}$ , which stands for the number of photons emitted by the sample;  $\int B_{Abs}$ , which stands for the number of photons absorbed by the sample; and  $\int B_{Provid}$ , which represents the number of excited light photons provided by the excitation light source. Among the calculated values,  $\eta_{IQE}$  has been introduced as the internal quantum efficiency, which is a reliable indicator of the sample's ability to convert excitation light energy into emission light. Notably, a higher value of  $\eta_{IQE}$  indicates a higher efficiency of the sample in emitting light [46,47]. Conversely, a higher value of  $\eta_{IQE}$  implies a higher thermal efficiency. Additionally,  $\eta_{EQE}$  denotes the external quantum efficiency, which reflects the actual photoluminescence strength of phosphor materials. It combines the internal quantum efficiency and absorption efficiency measures.

The study investigates the influence of calcination temperature on the quantum efficiency of  $\text{Eu}^{3+}$ -doped  $\text{Y}_2(\text{W}_x\text{Mo}_{1-x}\text{O}_4)_3$  powders, where  $x$  varies from 0 to 1 in increments of 0.25. The results are presented in Table 1. The quantum efficiency measured results of  $\text{Eu}^{3+}$ -doped  $\text{Y}_2(\text{W}_x\text{Mo}_{1-x}\text{O}_4)_3$  ( $x = 0, 0.25, 0.50, 0.75$ , and  $1.0$ ) reveal a decreasing trend in  $\eta_{IQE}$ , while the  $\eta_{EQE}$  initially increases and then decreases with an increase in calcination temperature. The observed reduction in  $\eta_{IQE}$  is attributed to two factors: (i) a decrease in the escape rate of excitation luminescence due to an increase in grain size, and (ii) an increase in surface defects. On the other hand, an increase in powder volume and the number of luminescent centers contributes to the enhancement of  $\eta_{IQE}$ . Interestingly, the tetragonal crystal structure exhibits higher quantum efficiency than the monoclinic crystal structure [48]. Based on a comprehensive analysis of the quantum efficiency of these samples, the  $\text{Eu}^{3+}$ -doped  $\text{Y}_2(\text{Mo}_{0.75}\text{W}_{0.25}\text{O}_4)_3$  powder calcined at  $900\text{ }^\circ\text{C}$  exhibits the highest quantum efficiency, with an  $\eta_{EQE}$  value of 0.32. This is much higher than the reported  $\eta_{EQE}$  of similar materials, such as 0.2238 ( $\text{Y}_2(\text{MoO}_4)_3:\text{Eu}^{3+}$ ) [30], 0.1278 ( $\text{CaMoO}_4:\text{Eu}^{3+}$ ) [49], and 0.1 ( $\text{Y}_2(\text{MoO}_4)_3:\text{Eu}^{3+}/\text{Au}$ ) [29]. These findings provide valuable insights into optimizing the synthesis conditions of luminescent materials for potential applications in optoelectronic devices.

**Table 1.** The quantum efficiency measured results of  $\text{Eu}^{3+}$ -doped  $\text{Y}_2(\text{W}_x\text{Mo}_{1-x}\text{O}_4)_3$  ( $x = 0, 0.25, 0.50, 0.75$ , and  $1.0$ ).

Samples	800 °C		900 °C		1000 °C	
	$\eta_{IQE}$	$\eta_{EQE}$	$\eta_{IQE}$	$\eta_{EQE}$	$\eta_{IQE}$	$\eta_{EQE}$
Mo1	0.95	0.21	0.93	0.25	0.91	0.26
Mo0.75	0.95	0.2	0.92	0.32	0.84	0.28
Mo0.5	0.91	0.13	0.88	0.16	0.85	0.14
Mo0.25	0.9	0.12	0.89	0.17	0.84	0.13
Mo0	0.9	0.11	0.88	0.15	0.85	0.14

## 2.6. Thermal Quenching

The phenomenon of temperature-dependent changes in the intensity of phosphor luminescence is a common occurrence in many industries [50,51]. It is widely accepted that the quenching limit for phosphor materials is reached when the luminescence intensity decreases to 80% of its value at room temperature with an increase in temperature. This temperature is known as the quenching temperature of the phosphor material. In this study, we present the measurement results for the quenching temperature of a sample

of  $\text{Eu}^{3+}$ -doped  $\text{Y}_2(\text{Mo}_{0.75}\text{W}_{0.25}\text{O}_4)_3$ , as shown in Figure 6. Since the thermal quenching behavior of all samples is similar, we focused our analysis on the representative case of  $\text{Mo}_{0.75}$ . Our findings provide valuable insights into the quenching temperature behavior of this particular phosphor material, which has important implications for future research in the field.

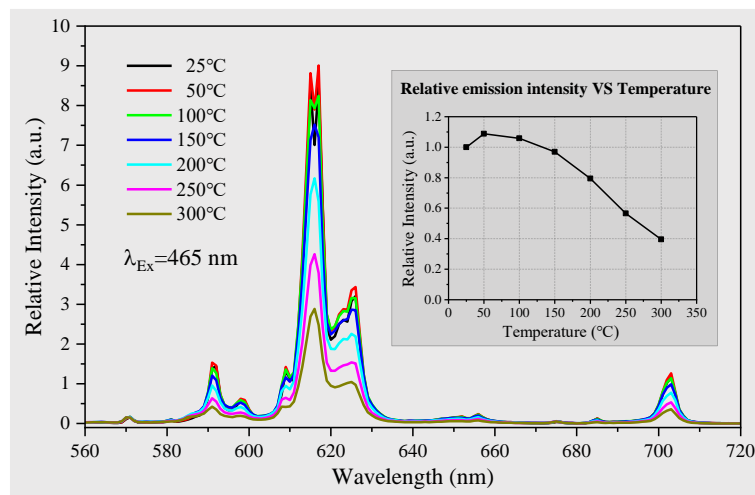


**Figure 6.** The emission spectra thermal quenching behavior of  $\text{YEu}(\text{Mo}_{0.75}\text{W}_{0.25}\text{O}_4)_3$  recorded under 465 nm; the illustration shows that the integral value of emission spectrum changes with the increase in temperature.

In this study, we conducted emission spectra measurements on a sample under 465 nm excitation light, while increasing the working temperature in steps of 50 °C from 25 °C to 300 °C. Our findings indicate that there is no discernible effect of temperature on the energy levels of  $\text{Eu}^{3+}$  ions, as evidenced by the lack of any change in the emission peaks position with increasing temperature. To explore the relationship between the integrated emission spectrum values of the  $\text{Mo}_{0.75}$  sample and working temperature, we generated the illustrated results shown in Figure 6. Our analysis reveals that the luminescence intensity of  $\text{Mo}_{0.75}$  sample first increases and then decreases with the increase in temperature. At around 50 °C, the luminescence intensity reaches its maximum, corresponding to a value of 1.1 times that at room temperature. This reason is that the probability of the electrons transition from the ground state to the excited state increases with the increase in temperature (the intensification of the thermal movement). However, as the temperature continues to rise, the luminescence intensity subsequently decreases. By the time the temperature reaches 150 °C, the luminescence intensity has essentially returned back to its original level at room temperature. The thermal quenching temperature of the sample was found to be 200 °C since at this point, the luminescence intensity had decreased to 80% of its value at room temperature. These results provide valuable insights into the precise mechanisms underlying the temperature-dependent behavior of phosphor material, which will help guide future research and applications in this field.

The phenomenon of thermal quenching is attributed to the absorption of heat energy by the electron in its excited state. This process leads to a transition to a higher energy level, the CTB (charge transfer band), which offers a nonradiative pathway for the electron [52,53]. Upon reaching the ground state, more heat is released, and this further increases the temperature, thereby creating a vicious cycle reminiscent of an avalanche effect. Elevating the working temperature of the phosphor material enhances the conversion of excitation energy into thermal energy, exacerbating the avalanche effect, and eventually leading to the triggering of the quenching temperature [50]. At this point, the temperature of the phosphor material rises rapidly, and its emission is quenched. These insights into the physical mechanism of thermal quenching have significant implications for understanding

the behavior of phosphor materials under changing temperature conditions and can guide future developments in this field [54].

### 3. Materials and Methods

#### 3.1. Synthesis

This study reports on the synthesis of a series of red phosphor powder samples, which are doped with  $\text{Eu}^{3+}$  in  $\text{Y}_2(\text{W}_x\text{Mo}_{1-x}\text{O}_4)_3$  ( $x = 0, 0.25, 0.50, 0.75, \text{ and } 1.0$ ), through a combination of an improved sol-gel process and high-temperature solid-state reaction method. The proportion of  $\text{Eu}^{3+}$  replacing  $\text{Y}^{3+}$  is 50%, and the molar concentration is about 6%. In the sol-gel process, citric acid was chosen as the chelating agent, with its molar amount being equivalent to the molar number of cations in the solution. The suspension solution was formed by adding yttrium nitrate (III), ammonium molybdate, europium nitrate (III), and tungstic acid into the citric acid solution. After being heated and stirred for 12–15 h, the water in the solution was evaporated, leaving a semi-solid gel behind. Subsequently, the semi-solid gel underwent calcination in a muffle furnace, experiencing solid-state reactions at high temperatures to form the desired red phosphor materials. These synthesized phosphors have potential applications in the field of solid-state lighting technology driven by their excellent photoluminescence properties.

#### 3.2. Characterization

We investigated the morphology, particle size, composition, and crystal structures of our samples through the use of Hitachi SU3500 for obtaining SEM images and EDS spectra. Our identification of crystal structures was based on X-ray diffraction patterns obtained from an Equinox1000 Sn.1612EQ1000137 diffractometer (Thermo Fisher; Horten, Norway), which utilized  $\text{Cu K}\alpha$  radiation ( $\lambda = 1.5418 \text{ \AA}$ ). Furthermore, we measured the emission and excitation spectra using an Edinburgh FS05 Fluorescence Spectrometer, and determined the quantum efficiency via a calibrated AvaSpec-ULS2048-EVO PL spectrometer and AvaSphere-50 integrating sphere. To assess thermal quenching temperature, our samples were heated with a HT24S-24W metal ceramic heater (ThorLabs). Photoluminescence relative intensity readings were taken at varying temperatures using the Edinburgh FS05 fluorescence spectrometer.

### 4. Conclusions

The synthesis of novel red phosphor powder materials,  $\text{Eu}^{3+}:\text{Y}_2(\text{W}_x\text{Mo}_{1-x}\text{O}_4)_3$  ( $x = 0, 0.25, 0.50, 0.75, \text{ and } 1.0$ ), was successfully achieved using an improved sol-gel process in combination with a high-temperature solid-state reaction method. The lattice structure of the samples was studied as a function of synthesis temperature and Mo/W ratio, and the photoluminescence performance of the resulting powders with varying lattice structures was evaluated. The monoclinic lattice structure was found to persist for  $x \leq 0.5$  regardless of calcination temperature, while the tetragonal crystal structure remained unchanged for  $x > 0.75$  at all calcination temperatures studied. For  $x = 0.75$ , the crystal structure transformed from tetragonal (800–900 °C) to monoclinic (1000 °C) depending on the calcination temperature. The photoluminescence efficiency of the tetragonal crystal structure was ~5% higher than that of the monoclinic crystal structure. A comprehensive analysis of the quantum efficiency of the samples showed that the  $\text{Eu}^{3+}$ -doped  $\text{Y}_2(\text{Mo}_{0.75}\text{W}_{0.25}\text{O}_4)_3$  sample calcined at 900 °C exhibited the highest quantum efficiency, with an external quantum efficiency of up to 0.32. In addition, the sample's measured thermal quenching temperature was found to be 200 °C, indicating that this material is highly promising for use in harsh environments and can withstand high excitation power density. These findings suggest that the new material could serve as a crucial component in the next generation of lighting technology, including laser lighting.

**Author Contributions:** Conceptualization, X.C. and M.N.A.; methodology, X.C., M.N.A. and F.C.; software, M.N.A.; validation, X.C., M.N.A. and F.C.; formal analysis, X.C., M.N.A. and F.C.; investigation, X.C. and M.N.A.; resources, X.C. and M.N.A.; data curation, F.C.; writing—original draft preparation, F.C.; writing—review and editing, X.C. and M.N.A.; visualization, X.C., M.N.A. and F.C.; supervision, X.C. and M.N.A.; project administration, X.C.; funding acquisition, X.C. All authors have read and agreed to the published version of the manuscript.

**Funding:** This research was funded by the Research Council of Norway FORNY RedOX project.

**Institutional Review Board Statement:** Not applicable.

**Informed Consent Statement:** Not applicable.

**Data Availability Statement:** More research data are available from the authors on request.

**Acknowledgments:** We would like to thank the laboratory engineers Zekija Ramic, Birgitte Kasin Hønsvall, and Muhammad Tayyib for their help. This work was also supported by the BIA Project HiLase of the Research Council of Norway and the Norwegian Micro- and Nano-Fabrication Facility.

**Conflicts of Interest:** The authors declare no conflict of interest.

**Sample Availability:** The reported samples are available from the authors on request.

## References

1. Höpfe, H. Recent Developments in the Field of Inorganic Phosphors. *Angew. Chem. (Int. Ed. Engl.)* **2009**, *48*, 3572–3582. [[CrossRef](#)] [[PubMed](#)]
2. Gaffuri, P.; Stolyarova, E.; Llerena, D.; Appert, E.; Consonni, M.; Robin, S.; Consonni, V. Potential substitutes for critical materials in white LEDs: Technological challenges and market opportunities. *Renew. Sustain. Energy Rev.* **2021**, *143*, 110869. [[CrossRef](#)]
3. Bispo, A.G., Jr.; Saraiva, L.F.; Lima, S.A.M.; Pires, A.M.; Davolos, M.R. Recent prospects on phosphor-converted LEDs for lighting, displays, phototherapy, and indoor farming. *J. Lumin.* **2021**, *237*, 118167. [[CrossRef](#)]
4. Qiao, J.; Zhao, J.; Liu, Q.; Xia, Z. Recent advances in solid-state LED phosphors with thermally stable luminescence. *J. Rare Earths* **2019**, *37*, 565–572. [[CrossRef](#)]
5. Ye, S.; Xiao, F.; Pan, Y.X.; Ma, Y.Y.; Zhang, Q.Y. Phosphors in phosphor-converted white light-emitting diodes: Recent advances in materials, techniques and properties. *Mater. Sci. Eng. R Rep.* **2010**, *71*, 1–34. [[CrossRef](#)]
6. Zhou, Z.; Xie, X.; Sun, Z.; Wang, X.; An, Z.; Huang, W. Recent Advances of Metal-free Phosphorescent Materials for Organic Light-emitting Diodes. *J. Mater. Chem. C* **2023**, *11*, 3143–3161. [[CrossRef](#)]
7. Li, G.; Tian, Y.; Zhao, Y.; Lin, J. Recent progress in luminescence tuning of Ce<sup>3+</sup> and Eu<sup>2+</sup>-activated phosphors for pc-WLEDs. *Chem. Soc. Rev.* **2015**, *44*, 8688–8713. [[CrossRef](#)] [[PubMed](#)]
8. Li, J.; Yan, J.; Wen, D.; Khan, W.U.; Shi, J.; Wu, M.; Su, Q.; Tanner, P.A. Advanced red phosphors for white light-emitting diodes. *J. Mater. Chem. C* **2016**, *4*, 8611–8623. [[CrossRef](#)]
9. Balci, M.; Chen, F.; Cunbul, A.; Svensen, Ø.; Akram, M.; Chen, X. Comparative study of blue laser diode driven cerium-doped single crystal phosphors in application of high-power lighting and display technologies. *Opt. Rev.* **2017**, *25*, 166–174. [[CrossRef](#)]
10. Lakde, J.; Mehare, C.M.; Pandey, K.K.; Dhoble, N.S.; Dhoble, S.J. Recent development of Eu<sup>3+</sup>-doped phosphor for white LED application: A review. *J. Phys. Conf. Ser.* **2021**, *1913*, 012029. [[CrossRef](#)]
11. Rajendran, M.; Vaidyanathan, S. High performance red/deep-red emitting phosphors for white LEDs. *New J. Chem.* **2020**, *44*, 5354–5365. [[CrossRef](#)]
12. Hu, Y.; Zhuang, W.; Ye, H.; Wang, D.; Zhang, S.; Huang, X. A novel red phosphor for white light emitting diodes. *J. Alloys Compd.* **2005**, *390*, 226–229. [[CrossRef](#)]
13. Li, Y.; Yang, Y.; Zheng, H.; Yu, F.; Liang, Q.; Yang, H.; Yi, X.; Wang, J.; Li, J. Review of High Power Phosphor-Converted Light-Emitting Diodes. In Proceedings of the 2019 16th China International Forum on Solid State Lighting & 2019 International Forum on Wide Bandgap Semiconductors China (SSLChina: IFWS), Shenzhen, China, 25–27 November 2019; pp. 111–115.
14. Shi, Y.; Cui, R.; Gong, X.; Deng, C. A novel red phosphor Ca<sub>2</sub>YNbO<sub>6</sub>: Eu<sup>3+</sup> for WLEDs. *Luminescence* **2022**, *37*, 1343–1351. [[CrossRef](#)] [[PubMed](#)]
15. Ahn, Y.N.; Kim, K.D.; Anoop, G.; Kim, G.S.; Yoo, J.S. Design of highly efficient phosphor-converted white light-emitting diodes with color rendering indices (R1 – R15) ≥ 95 for artificial lighting. *Sci. Rep.* **2019**, *9*, 16848. [[CrossRef](#)] [[PubMed](#)]
16. Luo, D.; Wang, L.; Or, S.W.; Zhang, H.; Xie, R.-J. Realizing superior white LEDs with both high R9 and luminous efficacy by using dual red phosphors. *RSC Adv.* **2017**, *7*, 25964–25968. [[CrossRef](#)]
17. Babu, J.; Sridhar, M.; Prasad, A.S.; Patrick, G.; Suresh, K. Novel red phosphor for LED applications. *Mater. Today Proc.* **2020**, *44*, 294–299. [[CrossRef](#)]
18. Lin, Y.-C.; Karlsson, M.; Bettinelli, M. Inorganic Phosphor Materials for Lighting. *Top. Curr. Chem.* **2016**, *374*, 309–355. [[CrossRef](#)]

19. Zhang, N.; Tsai, Y.T.; Fang, M.H.; Ma, C.G.; Lazarowska, A.; Mahlik, S.; Grinberg, M.; Chiang, C.Y.; Zhou, W.; Lin, J.G.; et al. Aluminate Red Phosphor in Light-Emitting Diodes: Theoretical Calculations, Charge Varieties, and High-Pressure Luminescence Analysis. *ACS Appl. Mater. Interfaces* **2017**, *9*, 23995–24004. [[CrossRef](#)]
20. Ye, W.; Zhao, C.; Shen, X.; Ma, C.; Deng, Z.; Li, Y.; Wang, Y.; Zuo, C.; Wen, Z.; Li, Y.; et al. High Quantum Yield Gd<sub>4.67</sub>Si<sub>3</sub>O<sub>13</sub>:Eu<sup>3+</sup> Red-Emitting Phosphor for Tunable White Light-Emitting Devices Driven by UV or Blue LED. *ACS Appl. Electron. Mater.* **2021**, *3*, 1403–1412. [[CrossRef](#)]
21. Adachi, S. Review—Mn<sup>4+</sup>-Activated Red and Deep Red-Emitting Phosphors. *ECS J. Solid State Sci. Technol.* **2019**, *9*, 1149. [[CrossRef](#)]
22. Wei, Y.; Xing, G.; Liu, K.; Li, G.; Dang, P.; Liang, S.; Liu, M.; Cheng, Z.; Jin, D.; Lin, J. New strategy for designing orangish-red-emitting phosphor via oxygen-vacancy-induced electronic localization. *Light Sci. Appl.* **2019**, *8*, 15. [[CrossRef](#)] [[PubMed](#)]
23. Binnemans, K. Interpretation of europium(III) spectra. *Coord. Chem. Rev.* **2015**, *295*, 1–45. [[CrossRef](#)]
24. Wang, C.; Zhang, S.; Ye, S. Investigation on thermal quenching of Eu<sup>3+</sup> luminescence in Sr<sub>2</sub>Ca(Mo/W)O<sub>6</sub>, Gd<sub>3</sub>B(Mo/W)O<sub>9</sub> and Ca(Mo/W)O<sub>4</sub>. *Ceram. Int.* **2021**, *47*, 13729–13737. [[CrossRef](#)]
25. Kong, L.; Sun, H.; Nie, Y.; Yan, Y.; Wang, R.; Ding, Q.; Zhang, S.; Yu, H.; Luan, G. Luminescent Properties and Charge Compensator Effects of SrMo<sub>0.5</sub>W<sub>0.5</sub>O<sub>4</sub>:Eu<sup>3+</sup> for White Light LEDs. *Molecules* **2023**, *28*, 2681. [[CrossRef](#)]
26. Du, P.; Yu, J.S. Eu<sup>3+</sup>-activated La<sub>2</sub>MoO<sub>6</sub>-La<sub>2</sub>WO<sub>6</sub> red-emitting phosphors with ultrabroad excitation band for white light-emitting diodes. *Sci. Rep.* **2017**, *7*, 11953. [[CrossRef](#)] [[PubMed](#)]
27. Neeraj, S.; Kijima, N.; Cheetham, A.K. Novel red phosphors for solid-state lighting: The system NaM(WO<sub>4</sub>)<sub>2-x</sub>(MoO<sub>4</sub>)<sub>x</sub>:Eu<sup>3+</sup> (M = Gd, Y, Bi). *Chem. Phys. Lett.* **2004**, *387*, 2–6. [[CrossRef](#)]
28. Chen, F.; Akram, M.N.; Chen, X. Improved Photoluminescence Performance of Eu<sup>3+</sup>-Doped Y<sub>2</sub>(MoO<sub>4</sub>)<sub>3</sub> Red-Emitting Phosphor via Orderly Arrangement of the Crystal Lattice. *Molecules* **2023**, *28*, 1014. [[CrossRef](#)]
29. Bispo, A., Jr.; Shinohara, G.; Pires, A.M.; Cardoso, C. Red phosphor based on Eu<sup>3+</sup>-doped Y<sub>2</sub>(MoO<sub>4</sub>)<sub>3</sub> incorporated with Au NPs synthesized via Pechini's method. *Opt. Mater.* **2018**, *84*, 137–145. [[CrossRef](#)]
30. Tian, Y.; Qi, X.; Wu, X.; Hua, R.; Chen, B. Luminescent Properties of Y<sub>2</sub>(MoO<sub>4</sub>)<sub>3</sub>:Eu<sup>3+</sup> Red Phosphors with Flowerlike Shape Prepared via Coprecipitation Method. *J. Phys. Chem. C* **2009**, *113*, 10767–10772. [[CrossRef](#)]
31. Wang, S.-Q.; Koteswara Rao, K.; Wang, Y.-R.; Hsu, Y.F.; Chen, S.-H.; Lu, Y.C. Structural Characterization and Luminescent Properties of a Red Phosphor Series: Y<sub>2-x</sub>Eu<sub>x</sub>(MoO<sub>4</sub>)<sub>3</sub> (x = 0.4–2.0). *J. Am. Ceram. Soc.* **2009**, *92*, 1732–1738. [[CrossRef](#)]
32. Tang, R.; Chen, H.; Yin, W.; Li, Y.; Ning, Z.; Zhong, C.; Zhao, Y.; Lai, X.; Bi, J.; Gao, D. Temperature-induced phase transition, luminescence and magnetic properties of Eu<sub>2</sub>(MoO<sub>4</sub>)<sub>3</sub> microcrystal red phosphors. *J. Mater. Sci. Mater. Electron.* **2019**, *30*, 7347–7358. [[CrossRef](#)]
33. Laufer, S.; Strobel, S.; Schleid, T.; Cybinska, J.; Mudring, A.-V.; Hartenbach, I. Yttrium(III) oxomolybdates(VI) as potential host materials for luminescence applications: An investigation of Eu<sup>3+</sup>-doped Y<sub>2</sub>[MoO<sub>4</sub>]<sub>3</sub> and Y<sub>2</sub>[MoO<sub>4</sub>]<sub>2</sub>[Mo<sub>2</sub>O<sub>7</sub>]. *New J. Chem.* **2013**, *37*, 1919–1926. [[CrossRef](#)]
34. Baur, F.; Jüstel, T. Eu<sup>3+</sup> Activated Molybdates—Structure Property Relations. *Opt. Mater. X* **2019**, *1*, 100015. [[CrossRef](#)]
35. Gates, S.D.; Lind, C. Polymorphism in yttrium molybdate Y<sub>2</sub>Mo<sub>3</sub>O<sub>12</sub>. *J. Solid State Chem.* **2007**, *180*, 3510–3514. [[CrossRef](#)]
36. Chen, G.; Wang, F.; Yu, J.; Zhang, H.; Zhang, X. Improved red emission by codoping Li<sup>+</sup> in ZnWO<sub>4</sub>:Eu<sup>3+</sup> phosphors. *J. Mol. Struct.* **2017**, *1128*, 1–4. [[CrossRef](#)]
37. Fang, Y.-C.; Chu, S.-Y.; Kao, P.-C.; Chuang, Y.-M.; Zeng, Z.-L. Energy Transfer and Thermal Quenching Behaviors of CaLa<sub>2</sub>(MoO<sub>4</sub>)<sub>4</sub>:Sm<sup>3+</sup>, Eu<sup>3+</sup> Red Phosphors. *J. Electrochem. Soc.* **2011**, *158*, J1–J5. [[CrossRef](#)]
38. Huang, Y.; Li, M.; Yang, L.; Zhai, B.-G. Eu<sup>2+</sup> and Eu<sup>3+</sup> Doubly Doped ZnWO<sub>4</sub> Nanoplates with Superior Photocatalytic Performance for Dye Degradation. *Nanomaterials* **2018**, *8*, 765. [[CrossRef](#)]
39. Chen, F.; Balci, M.; Xia, H.; Akram, M.; Chen, X. Photoluminescence Properties and Quantum Efficiency of Eu<sup>3+</sup>/Mn<sup>2+</sup>-Doped ZnMoO<sub>4</sub> Red Phosphor. *Key Eng. Mater.* **2020**, *843*, 70–78. [[CrossRef](#)]
40. Ran, W.; Noh, H.; Park, S.H.; Moon, B.; Jeong, J.; Kim, J.; Shi, J. Break the Interacting Bridge between Eu<sup>3+</sup> Ions in the 3D Network Structure of CdMoO<sub>4</sub>:Eu<sup>3+</sup> Bright Red Emission Phosphor. *Sci. Rep.* **2018**, *8*, 5936. [[CrossRef](#)]
41. Zhang, L.; Xu, Y.; Wu, X.; Yin, S.; You, H. Strong and pure red-emitting Eu<sup>3+</sup>-doped phosphor with excellent thermal stability for warm WLEDs. *Mater. Adv.* **2022**, *3*, 2591–2597. [[CrossRef](#)]
42. Zhang, S.; Nakai, Y.; Tsuboi, T.; Huang, Y.; Seo, H.J. Luminescence and Microstructural Features of Eu-Activated LiBaPO<sub>4</sub> Phosphor. *Chem. Mater.* **2011**, *23*, 1216–1224. [[CrossRef](#)]
43. Chen, F.; Akram, M.N.; Chen, X. Nanocomposite phosphor materials fabricated by solid-state reaction for optoelectronics application. In Proceedings of the 2020 IEEE 8th Electronics System-Integration Technology Conference (ESTC), Tonsberg, Norway, 15–18 September 2020; pp. 1–4.
44. Binnemans, K. Lanthanide-Based Luminescent Hybrid Materials. *Chem. Rev.* **2009**, *109*, 4283–4374. [[CrossRef](#)] [[PubMed](#)]
45. Reisfeld\*, R.; Zigansky, E.; Gaft, M. Europium probe for estimation of site symmetry in glass films, glasses and crystals. *Mol. Phys.* **2004**, *102*, 1319–1330. [[CrossRef](#)]
46. Kodaira, C.A.; Brito, H.F.; Malta, O.L.; Serra, O.A. Luminescence and energy transfer of the europium (III) tungstate obtained via the Pechini method. *J. Lumin.* **2003**, *101*, 11–21. [[CrossRef](#)]
47. Qin, X.; Liu, X.; Huang, W.; Bettinelli, M.; Liu, X. Lanthanide-Activated Phosphors Based on 4f-5d Optical Transitions: Theoretical and Experimental Aspects. *Chem. Rev.* **2017**, *117*, 4488–4527. [[CrossRef](#)]

48. Qiao, J.; Xia, Z. Design principles for achieving red emission in  $\text{Eu}^{2+}/\text{Eu}^{3+}$  doped inorganic solids. *J. Appl. Phys.* **2021**, *129*, 200903. [[CrossRef](#)]
49. Lei, F.; Yan, B. Hydrothermal synthesis and luminescence of  $\text{CaMoO}_4:\text{RE}^{3+}$  ( $\text{M} = \text{W}, \text{Mo}$ ;  $\text{RE} = \text{Eu}, \text{Tb}$ ) submicro-phosphors. *J. Solid State Chem.* **2008**, *181*, 855–862. [[CrossRef](#)]
50. Chen, Z.; Cao, C.; Zhang, M.; Huang, N.; Bai, B.; Yang, L.; Li, Y.; Xie, A. Thermal enhancing photoluminescence intensities of  $\text{Eu}^{3+}$  doped  $\text{Lu}_2(\text{MoO}_4)_3$ . *Opt. Mater.* **2022**, *127*, 112301. [[CrossRef](#)]
51. Zhuo, Y.; Hariyani, S.; Armijo, E.; Abolade Lawson, Z.; Brgoch, J. Evaluating Thermal Quenching Temperature in  $\text{Eu}^{3+}$ -Substituted Oxide Phosphors via Machine Learning. *ACS Appl. Mater. Interfaces* **2020**, *12*, 5244–5250. [[CrossRef](#)]
52. Janulevicius, M.; Marmokas, P.; Misevicius, M.; Grigorjevaite, J.; Mikoliunaite, L.; Sakirzanovas, S.; Katelnikovas, A. Luminescence and luminescence quenching of highly efficient  $\text{Y}_2\text{Mo}_4\text{O}_{15}:\text{Eu}^{3+}$  phosphors and ceramics. *Sci. Rep.* **2016**, *6*, 26098. [[CrossRef](#)]
53. Dang, P.; Li, G.; Yun, X.; Zhang, Q.; Liu, D.; Lian, H.; Shang, M.; Lin, J. Thermally stable and highly efficient red-emitting  $\text{Eu}^{3+}$ -doped  $\text{Cs}_3\text{GdGe}_3\text{O}_9$  phosphors for WLEDs: Non-concentration quenching and negative thermal expansion. *Light Sci. Appl.* **2021**, *10*, 29. [[CrossRef](#)] [[PubMed](#)]
54. He, X.; Bian, D.; Wang, H.; Xu, J.  $\text{Eu}^{3+}$ -activated  $\text{Y}_2\text{MoO}_6$ : A narrow band red-emitting phosphor with strong near-UV absorption. *Lumin. J. Biol. Chem. Lumin.* **2012**, *28*, 973–976. [[CrossRef](#)] [[PubMed](#)]

**Disclaimer/Publisher’s Note:** The statements, opinions and data contained in all publications are solely those of the individual author(s) and contributor(s) and not of MDPI and/or the editor(s). MDPI and/or the editor(s) disclaim responsibility for any injury to people or property resulting from any ideas, methods, instructions or products referred to in the content.